Letter

1*s*2*p* resonant inelastic x-ray scattering natural circular dichroism

James M. Ablett [1,*] Nazanin Kordestani [2] Amélie Juhin [3] Alessandro De Frenza [3] Marie-Anne Arrio [3] Patrick Rosa [2] Elen Duverger-Nédellec [2] Edwige Otero [1] Jean-Pascal Rueff [1,4] Philippe Sainctavit [1,3] and Elizabeth A. Hillard [2]

[1] *Synchrotron SOLEIL, L'Orme des Merisiers, Départementale 128, 91190 Saint-Aubin, France*
[2] *Université Bordeaux, CNRS, Bordeaux INP, ICMCB, UMR 5026, F-33600 Pessac, France*
[3] *CNRS, Sorbonne Université MNHN, IMPMC UMR 7590, F-75252 Paris, France*
[4] *Laboratoire de Chimie Physique-Matière et Rayonnement, CNRS, UMR 7614, Sorbonne Université, 4 Place Jussieu, 75252 Paris, France*

(Received 26 August 2025; revised 15 February 2026; accepted 23 March 2026; published 21 April 2026)

Natural circular dichroism (NCD) provides fundamental insight into molecular chirality and stereochemical environments. Extending this concept into the hard-x-ray regime enables element-specific and site-selective chiral sensitivity inaccessible to optical wavelengths. Here, we demonstrate that 1*s*2*p* resonant inelastic x-ray scattering (RIXS) can be used to probe NCD in the enantiomeric model compound $[Co(en)_3](NO_3)_2$. Using high-resolution detection of Co $K\alpha$ emission under circularly polarized excitation at the cobalt 1*s* pre-edge, we observe pronounced dichroic behavior directly linked to the Co-centered chirality. The RIXS-NCD signal reaches $\approx 23\%$ of the pre-edge maximum—more than twice the amplitude of the previously reported x-ray NCD signal for the same compound—and exhibits the expected angular dependence for the crystal's $P6_322$ symmetry. Two-dimensional RIXS-NCD maps further reveal strong helicity-dependent features across both excitation and emission energies, providing a richer description of the chiral electronic structure. These results establish RIXS-NCD as a photon-in–photon-out methodology for investigating natural optical activity with elemental and orbital specificity, paving the way for future applications to complex chiral and bioinspired materials.

DOI: 10.1103/pgjx-znm3

Natural circular dichroism (NCD)—the differential absorption of left- and right-handed circularly polarized light—is a cornerstone technique for probing molecular chirality [1]. Conventional optical and infrared NCD provide information on the electronic and vibrational transitions of chiral molecules, but they are limited by the often delocalized nature of optical transitions and by the lack of element selectivity. In contrast, x-ray natural circular dichroism (XNCD) offers site-specific access to the chiral electronic structure by exploiting the interference between electric dipole (E1) and electric quadrupole (E2) transitions near an absorption edge in ordered media [2,3]. Hard x-ray XNCD has been successfully demonstrated at several synchrotron facilities, including the European Synchrotron Research Facility (ESRF) [4–15] and the Advanced Photon Source (APS) [16], typically at the *K* edges of transition metals or the *L* edges of heavier elements such as iodine [4] and lanthanides [12–15]. These experiments have revealed that hard x-rays offer true bulk sensitivity, minimal birefringence, and compatibility with *in situ* environments—advantages that make x-ray chiroptical methods particularly appealing for condensed-phase materials studies. Yet, despite these advances, conventional XNCD remains a one-dimensional probe: it measures only absorption differences and is thus limited by the natural linewidths of deep-core holes and by diffraction peaks that can mask weak dichroic signals.

Resonant inelastic x-ray scattering (RIXS) provides a way to overcome these limitations. As an energy-resolved, photon-in–photon-out technique, RIXS simultaneously probes the absorption and emission channels of a core-excited system, revealing element- and orbital-specific information with sub-eV resolution [17]. In 1*s*2*p* RIXS on first row transition-metal complexes, excitation of a 1*s* electron into unoccupied 3*d* and 4*p* orbitals is followed by $2p \rightarrow 1s$ emission, producing spectra that reflect the local symmetry, oxidation state, and ligand field of the absorbing atom [18]. The reduced lifetime broadening of the 2p core-hole in the final state and the suppression of diffraction peaks, and elastic and fluorescence backgrounds by spherical crystal analyzers (SCAs), make RIXS ideally suited for detecting subtle dichroic effects [17,19–22].

In this work, we present an experimental demonstration of RIXS-NCD using the enantiomeric model system $[Co(en)_3](NO_3)_2$. This compound, which crystallizes in the space group $P6_322$, has previously shown measurable XNCD at the Co *K* pre-edge, making it an ideal reference for comparison [23]. Single crystals of Δ- and Λ-$[Co(en)_3](NO_3)_2$ were prepared following established protocols [24] and their handedness verified by single-crystal x-ray diffraction. Experiments were carried out at the GALAXIES beamline of the SOLEIL synchrotron [25], using circularly polarized (CP) hard x-rays, with P_c close to 100%, generated by a quarter-wave plate [26] and monochromatized by a Si(111) double-crystal monochromator. The helicity was alternated at each energy step, and the incident beam was focused to a

*Contact author: james.ablett@synchrotron-soleil.fr

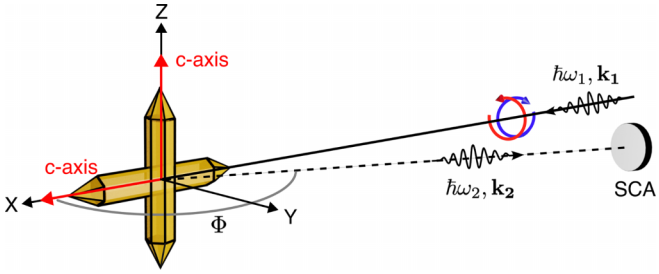

FIG. 1. Perspective view of the experimental geometry for RIXS-NCD. Incident CP x-rays, denoted by the red and blue circular arrows, of energy $\hbar\omega_1$ are oriented parallel (axial) or perpendicular (orthoaxial) to the crystal optical axis. The SCA selects the emitted x-rays of energy $\hbar\omega_2$ at a scattering angle Φ (in the horizontal scattering plane) relative to the incident x-ray beam and focuses them onto a silicon drift detector (not shown).

30[vertical]×90 [horizontal] μm^2 spot on the sample under a helium atmosphere. The experimental geometry is shown in Fig. 1: the crystals were orientated such that the incident beam was either parallel (axial geometry) or perpendicular (orthoaxial geometry) to the crystallographic c axis. The emitted photons were energy analyzed by a single 1 m radius Si(531) spherical crystal analyzer positioned in the horizontal scattering plane at $\Phi = 135°$ or 145° and tuned to the Co $K\alpha_1$ emission line. To avoid beam damage, the x-ray intensity was reduced from its maximum value of $\approx 2 \times 10^{13}$ photons/s to $\approx 2 \times 10^{10}$ photons/s, and the sample position was frequently refreshed. Detailed experimental procedures can be found in the accompanying Supplemental Material [27].

Figure 2(a) displays representative high-energy-resolved fluorescence-detected (HERFD) x-ray absorption spectroscopy (XAS) spectra at the Co K edge recorded with opposite helicities, showing a clear pre-edge dichroism. The corresponding HERFD-NCD spectra [Fig. 2(b)] reveal mirror-image behavior for the Δ and Λ enantiomers. The

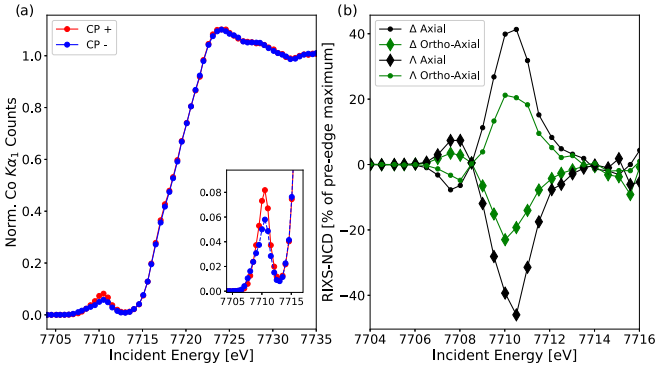

FIG. 2. (a) Representative HERFD-XAS spectra on Δ axial $[Co(en)_3](NO_3)_2$ at the Co K edge recorded with alternating helicities (CP^+, CP^-) with the emission energy set to the maximum of the Co $K\alpha_1$ line. Inset: zoom in on the Co 1s pre-edge dichroism. (b) HERFD-NCD spectra for both enantiomers of $[Co(en)_3](NO_3)_2$. For these data, the crystals were arranged in either axial or orthoaxial geometries and the incident energy scanned across the Co 1s pre-edge with alternating helicities with the spectrometer emission energy set to the maximum of the Co $K\alpha_1$ line. The HERFD-NCD signal was simply obtained by taking the difference between these two datasets.

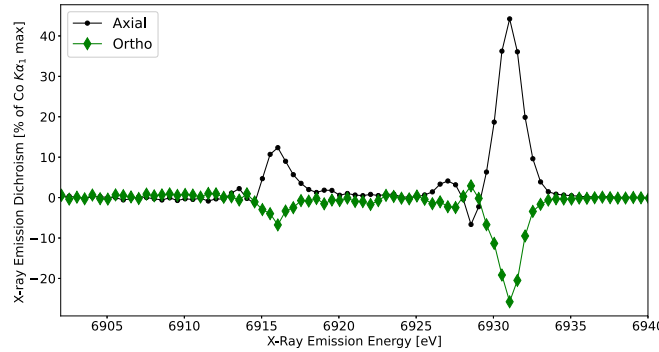

FIG. 3. XES-NCD taken on Δ-$[Co(en)_3](NO_3)_2$, in both axial and orthoaxial geometries, at an incident x-ray energy of 7710 eV corresponding to the maximum of the HERFD-NCD signal. The data were obtained by scanning the spectrometer x-ray emission energy across the Co $K\alpha_1$ and $K\alpha_2$ emission lines for alternating helicities. The helicities were flipped after each complete x-ray emission scan, and the dichroic x-ray emission spectrum obtained from their difference, expressed as a percentage of the average Co $K\alpha_1$ maximum intensity.

dichroic signal is maximal at the Co $1s \rightarrow 3d/4p$ pre-edge and reaches ≈ 23% of the pre-edge intensity—more than twice the 9.6% amplitude previously observed in XNCD [23]. The signal reverses sign and decreases by roughly a factor of 2 between the axial and orthoaxial geometries, following the expected $3\cos^2\theta - 1$ angular dependence for D_6 crystal symmetry [30]. These results unambiguously demonstrate the presence of natural circular dichroism in a chiral system probed by RIXS-NCD.

To explore the emission dependence, we performed x-ray emission spectroscopy (XES) at a fixed excitation energy corresponding to the maximum dichroic response ($\hbar\omega_1 \approx$ 7710 eV). Figure 3 shows the difference between these spectra taken with alternating helicities, and for both the axial and orthoaxial geometries. In these XES-NCD spectra, both the Co $K\alpha_1$ ($2p_{3/2} \rightarrow 1s$) and $K\alpha_2$ ($2p_{1/2} \rightarrow 1s$) emission lines exhibit helicity-dependent intensity variations with the same sign for Δ-$[Co(en)_3](NO_3)_2$, as expected for a nonmagnetic chiral effect [4]. The magnitude of the helicity-dependent modulation in the $K\alpha_1$ line reaches ≈ 44% of its mean intensity in the axial geometry, making it one of the strongest circular dichroic signals reported for a chiral system in the hard x-ray regime.

Two-dimensional RIXS-NCD maps, obtained by recording full emission spectra as a function of incident energy for both helicities, provide a complete picture of the phenomenon (Fig. 4). The polarization-averaged map shows the main $1s2p$ resonant features, while the dichroic map reveals broad regions of helicity-dependent intensity over several electron volts in both excitation and emission dimensions. The extended dichroic structure indicates that multiple intermediate states contribute coherently to the overall response. Line profiles extracted from these maps (Fig. 5) confirm that the dichroic contrast evolves systematically across the pre-edge and emission regions, maintaining the same sign and symmetry as the one-dimensional spectra. The maximum RIXS-NCD signal is found to occur around 6931.3 eV, with a similar spectral weight between the dichroic features at ≈7708 eV

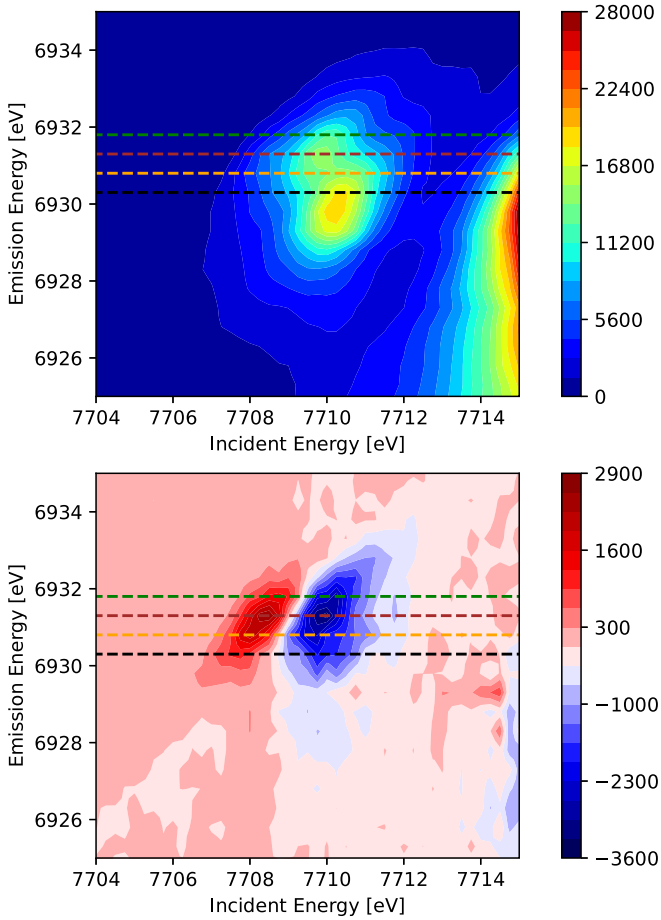

FIG. 4. Top: A "polarization-independent" RIXS map on Δ-$[Co(en)_3](NO_3)_2$ in orthoaxial orientation. The map was taken by scanning the emission energy across the Co $K\alpha_1$ emission line at each incident x-ray energy with alternating helicity (CP^+, CP^-). The data were summed for each polarization and divided by 2, to mimic a polarization-independent RIXS map. Bottom: The RIXS-NCD map obtained from the difference between the polarization-dependent spectra used in the top panel. A clear dichroism is observed over several eV in incident and emission energies in the Co 1*s* pre-edge region. The horizontal dashed lines indicate x-ray emission energies used to plot the HERFD-XAS and HERFD-NCD spectra in Fig. 5.

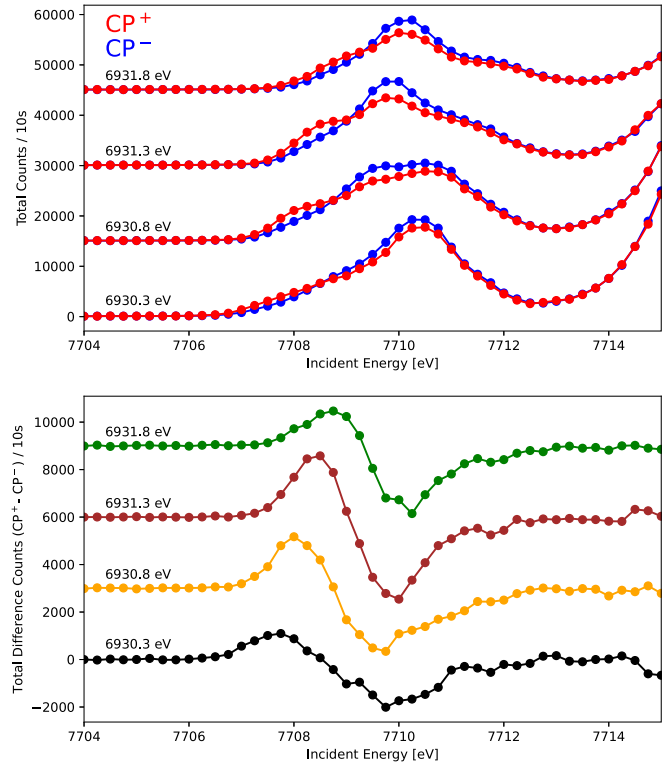

FIG. 5. Top: Polarization-dependent (CP^+, CP^-) HERFD-XAS spectra taken from Fig. 4 at specific x-ray emission energies. Bottom: HERFD-NCD spectra obtained from the difference between the two polarization datasets presented in the top panel.

and ≈7710 eV. The RIXS-NCD signal at 6930.3 eV resembles that shown in Fig. 2(b), recorded at approximately the same emission energy and showing a strong intensity difference between these two dichroic features. This clearly indicates that RIXS-NCD is substantially richer than XNCD, for which both theory and experiment have demonstrated the existence of only a single dichroic line shape in D_6 symmetry.

The physical origin of the observed RIXS-NCD can be understood in terms of the interference between E1 and E2 transition amplitudes in the intermediate state of the RIXS process. The RIXS scattering amplitude can be written in the standard Kramers-Heisenberg form (see, e.g., Refs. [17,31]):

$$I(\omega_1,\omega_2) \propto \sum_f \left| \sum_n \frac{\langle f|\hat{O}_{2p\to 1s}|n\rangle\langle n|\hat{O}_{1s\to 3d,4p}|i\rangle}{E_i - E_n + \hbar\omega_1 + i\Gamma_n/2} \right|^2 \times \delta(E_f - E_i - \hbar\omega_1 + \hbar\omega_2),$$

where $|i\rangle, |n\rangle, |f\rangle$ denote the initial, intermediate and final states with energies E_i, E_n, E_f; $\hbar\omega_1$ and $\hbar\omega_2$ are the incoming and outgoing photon energies; $\hat{O}_{1s\to 3d,4p}$ and $\hat{O}_{2p\to 1s}$ are the absorption and emission operators, respectively; Γ_n is the intermediate-state lifetime broadening; and the interference between the E1 and E2 terms in $\hat{O}_{1s\to 3d,4p}$ gives rise to the observed helicity dependence. The stronger dichroic contrast observed in RIXS-NCD compared with XNCD results from (i) the narrower lifetime broadening of the 2*p* final state, (ii) the background suppression achieved by energy-resolved emission detection, and (iii) the coherent coupling between excitation and decay channels that amplifies the E1–E2 interference term.

A useful comparison can be made with RIXS–magnetic circular dichroism (RIXS-MCD) at the *K* pre-edge of 3*d* elements [18,32,33], though with the difference that RIXS-MCD arises in magnetically ordered materials from E1.E1 and E2.E2 terms in the absorption process. In systems such as Fe_3O_4 [32] and CrO_2 [18], RIXS-MCD signals were found to exceed *K*-edge XMCD by an order of magnitude. The present RIXS-NCD data show also a strong enhancement but in a purely nonmagnetic, structurally chiral system, demonstrating the generality of RIXS dichroism as a probe of broken symmetries.

In conclusion, we have demonstrated that 1*s*2*p* RIXS-NCD provides a sensitive and robust means of detecting natural circular dichroism in nonmagnetic chiral materials. The RIXS-NCD amplitude in $[Co(en)_3](NO_3)_2$ exceeds

that of conventional XNCD by more than a factor of 2 and exhibits the angular dependence expected from crystal symmetry. The two-dimensional RIXS-NCD maps reveal extended helicity-dependent features across both excitation and emission energies, reflecting coherent multipole interference. These findings establish RIXS-NCD as a powerful tool for element- and site-selective studies of chirality in solids.

Looking forward, the multidimensional nature of RIXS-NCD opens promising avenues for investigating chiral electronic structure, orbital hybridization, and symmetry-breaking interactions in complex systems. The development of RIXS-NCD sum rules and tensorial formalisms [34], analogous to those of XNCD [30] and RIXS [35], will enable quantitative connection between dichroic intensities and the multipole moments of chiral electronic densities. Extending this approach to transition-metal and lanthanide systems with strong spin-orbit coupling may provide insight into the coupling between chirality, orbital polarization, and magnetism.

We acknowledge N. Daro and G. Chastanet for laboratory management and S. Pechev for x-ray crystallography service management. We gratefully appreciate fruitful discussions with C. Brouder, A. Rogalev, F. Wilhelm, and P. Ohresser. Enormous gratitude goes to S. Gliga, J. Harrison, and M. Sikora, who helped with the setup and use of their portable quarter-wave plate that was used for obtaining the RIXS-NCD maps due to the motor failure of the GALAXIES instrument.

The authors acknowledge ANR XIMTEX (Grant No. PRC ANR-21-CE29-0032), ANR CAORSS (Grant No. PRC ANR-21-CE29-0006), and the Synchrotron SOLEIL (Projects No. 99220073, No. 99230179, and No. 99240043) for financial assistance. This work is part of the LUMINESS project of the PEPR LUMA and has received support from the French government, managed by the National Research Agency under the France 2030 program, with Reference No. ANR-24-EXLU-0006.

Conceptualization: J.M.A., E.A.H., and P.S.; Funding acquisition: J.M.A., E.A.H., and P.S.; Investigation: J.M.A., M.-A.A., E.A.H., A.J., E.D.-N., N.K., P.R., P.S., A.D.F., E.O., and J.-P.R.; Validation: J.M.A., E.A.H., and P.S.; Project administration: J.M.A., E.A.H., and P.S.; Supervision: J.M.A., E.A.H., P.R., and P.S.; Writing original draft: J.M.A., E.A.H., A.J., and P.S.; Writing review: all authors.

Data availability. The data that support the findings of this article are openly available [36].

[1] N. Berova, P. Polavarapu, K. Nakanishi, and R. Woody, *Comprehensive Chiroptical Spectroscopy: Applications in Stereochemical Analysis of Synthetic Compounds, Natural Products, and Biomolecules* (John Wiley and Sons, Hoboken, New Jersey, 2012).

[2] J. Goulon, C. Goulon-Ginet, A. Rogalev, G. Benayoun, C. Brouder, and C. Natoli, X-ray natural circular dichroism and chiral-EXAFS in gyrotropic crystals, J. Synchrotron. Radiat. **7**, 182 (2000).

[3] J. Goulon, A. Rogalev, F. Wilhelm, N. Jaouen, C. Goulon-Ginet, and C. Brouder, Optical activity probed with x-rays, J. Phys.: Condens. Matter **15**, S633 (2003).

[4] J. Goulon, C. Goulon-Ginet, A. Rogalev, V. Gotte, C. Malgrange, C. Brouder, and C. Natoli, X-ray natural circular dichroism in a uniaxial gyrotropic single crystal of LiO_3, J. Chem. Phys. **108**, 6394 (1998).

[5] B. Stewart, R. Peacock, L. Alagna, T. Prosperi, S. Turchini, J. Goulon, A. Rogalev, and C. C. Goulon-Ginet, Circular dichroism at the edge: Large x-ray natural CD in the 1s → 3d pre-edge feature of $2[Co(en)_3Cl_3] \cdot NaCl \cdot 6H_2O$, J. Am. Chem. Soc. **121**, 10233 (1999).

[6] R. Sessoli, M.-E. Boulon, A. Caneschi, M. Mannini, L. Poggini, F. Wilhelm, and A. Rogalev, Strong magneto-chiral dichroism in a paramagnetic molecular helix observed by hard X-rays, Nat. Phys. **11**, 69 (2015).

[7] A. Srinivasan, M. Cortijo, V. Bulicanu, A. Naim, R. Clerac, P. Sainctavit, A. Rogalev, F. Wilhelm, P. Rosa, and E. Hillard, Enantiomeric resolution and x-ray optical activity of a tricobalt extended metal atom chain, Chem. Sci. **9**, 1136 (2018).

[8] E. Ovchinnikova, A. Rogalev, F. Wilhelm, K. Kozlovskaya, A. Oreshko, and V. Dmitrienko, X-ray natural circular dichroism in copper metaborate, J. Exp. Theor. Phys. **123**, 27 (2016).

[9] M. N. Norman, X-ray natural dichroism and chiral order in underdoped cuprates, Phys. Rev. B **87**, 180506(R) (2013).

[10] A. Rogalev, J. Goulon, F. F. Wilhelm, K. Kozlovskaya, E. Ovchin-nikova, L. Soboleva, A. Konstantinova, and V. Dmitrienko, Investigation of X-ray natural circular dichroism in a $CsCuCl_3$ single crystal: Theory and experiment, Crystallogr. Rep. **53**, 384 (2008).

[11] U. Serdan, L. Robin, M. Marchivie, M. Gonidec, P. Rosa, E. Duverger-Nédellec, E. Pouget, P. Sainctavit, M.-A. Arrio, A. Juhin, A. Rogalev, F. Wilhelm, and E. Hillard, Crystal engineering of conglomerates: Dilution of racemate-forming Fe(II) and Ni(II) congeners into conglomerate-forming $[Zn(bpy)_3](PF_6)_2$, Chemistry **5**, 255 (2023).

[12] I. Mihalcea, M. Perfetti, F. Pineider, L. Tesi, V. Mereacre, F. Wilhelm, A. Rogalev, C. Anson, A. Powell, and R. Sessoli, Spin helicity in chiral lanthanide chains, Inorg. Chem. **55**, 10068 (2016).

[13] L. Alagna, T. Prosperi, S. Turchini, J. Goulon, A. Rogalev, C. Goulon-Ginet, C. R. Natoli, R. D. Peacock, and B. Stewart, X-Ray natural circular dichroism, Phys. Rev. Lett. **80**, 4799 (1998).

[14] A. Oreshko, E. Ovchinnikova, A. Rogalev, F. Wilhelm, B. Mill, and V. Dmitrienko, X-ray natural circular dichroism in langasite crystal, J Synchrotron Radiat. **25**, 222 (2018).

[15] A. Oreshko, B. Mill, E. Ovchinnikova, A. Rogalev, F. Wilhelm, and V. Dmitrienko, X-Ray natural circular dichroism in langasite crystal at the Ga and La edges, Crystallogr. Rep. **63**, 158 (2018).

[16] D. Haskel, C. C. Won, Y. Joly, J. Strempfer, G. Fabbris, and S.-W. Cheong, Deconvolution of x-ray natural and magnetic circular dichroism in chiral dy-ferroborate, Sci. Rep. **14**, 24453 (2024).

[17] F. de Groot, M. Haverkort, H. Elnaggar, A. Juhin, K.-J. Zhou, and P. Glatzel, Resonant inelastic X-ray scattering, Nat. Rev. Methods Primers **4**, 45 (2024).

[18] P. Zimmermann, N. Bouldi, M. Hunault, M. Sikora, J. Ablett, J.-P. Rueff, B. Lebert, P. Sainctavit, F. de Groot, and A. Juhin, 1s2p resonant inelastic X-ray scattering magnetic circular dichroism as a probe for the local and non-local orbitals in CrO_2, J. Electron Spectrosc. Relat. Phenom. **222**, 74 (2018).

[19] J. Swarbrick, U. Skyllberg, and T. K. P. Glatzel, High energy resolution X-ray absorption spectroscopy of environmentally relevant lead(II) compounds, Inorg. Chem. **48**, 10748 (2009).

[20] F. M. F. de Groot, M. H. Krisch, and J. Vogel, Spectral sharpening of the Pt L edges by high-resolution x-ray emission, Phys. Rev. B **66**, 195112 (2002).

[21] A. Juhin, P. Sainctavit, K. Ollefs, M. Sikora, A. Filipponi, P. Glatzel, F. Wilhelm, and A. Rogalev, X-ray magnetic circular dichroism measured at the Fe K-edge with a reduced intrinsic broadening: X-ray absorption spectroscopy versus resonant inelastic X-ray scattering measurements, J. Phys.: Condens. Matter **28**, 505202 (2016).

[22] K. Hämäläinen, D. P. Siddons, J. B. Hastings, and L. E. Berman, Elimination of the inner-shell lifetime broadening in x-ray-absorption spectroscopy, Phys. Rev. Lett. **67**, 2850 (1991).

[23] M. Cortijo, A. Valentín-Pérez, A. Rogalev, F. Wilhelm, P. Sainctavit, P. Rosa, and E. Hillard, Rapid Discrimination of crystal handedness by X-ray natural circular dichroism (XNCD) mapping, Chem. A European J **26**, 13363 (2020).

[24] M. Cortijo, A. Valentín-Pérez, M. Rouzières, R. Clérac, P. Rosa, and E. Hillard, Tris(ethylenediamine) cobalt(II) and manganese(II) nitrates, Crystals **10**, 472 (2020).

[25] J. Ablett, D. Prieur, D. Céolin, B. Lassalle-Kaiser, B. Lebert, M. Sauvage, T. Moreno, S. Bac, V. Balédent, A. Ovono, M. Morand, F. Gélebart, A. Shukla, and J.-P. Rueff, The GALAXIES inelastic hard X-ray scattering end-station at synchrotron SOLEIL, J. Synchrotron Radiat. **26**, 263 (2019).

[26] L. Manzanillas, J. M. Ablett, M. Choukroun, F. J. Iguaz, and J.-P. Rueff, Development of an X-ray polarimeter at the SOLEIL synchrotron, Rev. Sci. Instrum. **95**, 053302 (2024).

[27] See Supplemental Material at http://link.aps.org/supplemental/10.1103/pgjx-znm3 for details on the experimental procedures, the operation of the quarter-wave plates for generating circular polarization, and the scanning parameters used for data acquisition, which also includes Refs. [28,29].

[28] A. Thompson, D. Attwood, E. Gullikson, M. Howells, K.-J. Kim, J. Kirz, J. Kortright, I. Lindau, P. Pianetta, A. Robinson, J. Scofield, J. Underwood, D. Vaughan, G. Williams, and H. Winnick, *X-Ray Data Booklet* (Lawrence Berkeley National Laboratory, University of California, Berkeley, CA, 2009).

[29] S. Pizzini, M. Bon, F. Baudelet, H. Tolentino, A. S. Miguel, K. Mackay, C. Malgrange, M. Hagelstein, and A. Fontaine, Quarter-wave plates and X-ray magnetic circular dichroism on ID24 at the ESRF, J Synchrotron Radiat. **5**, 1298 (1998).

[30] C. R. Natoli, C. Brouder, P. Sainctavit, J. Goulon, C. Goulon-Ginet, and A. Rogalev, Calculation of x-ray natural circular dichroism, Eur. Phys. J. B **4**, 1 (1998).

[31] L. J. P. Ament, M. van Veenendaal, T. P. Devereaux, J. P. Hill, and J. van den Brink, Resonant inelastic x-ray scattering studies of elementary excitations, Rev. Mod. Phys. **83**, 705 (2011).

[32] M. Sikora, A. Juhin, T.-C. Weng, P. Sainctavit, C. Detlefs, F. de Groot, and P. Glatzel, Strong K-edge magnetic circular dichroism observed in photon-in–photon-out spectroscopy, Phys. Rev. Lett. **105**, 037202 (2010).

[33] N. Daffé, J. Zečević, K. N. Trohidou, M. Sikora, M. Rovezzi, C. Carvallo, M. Vasilakaki, S. Neveu, J. D. Meeldijk, N. Bouldi, V. Gavrilov, Y. Guyodo, F. Choueikani, V. Dupuis, D. Taverna, P. Sainctavit, and A. Juhin, Bad neighbour, good neighbour: How magnetic dipole interactions between soft and hard ferrimagnetic nanoparticles affect macroscopic magnetic properties in ferrofluids, Nanoscale **12**, 11222 (2020).

[34] A. Juhin, C. Brouder, and F. de Groot, Angular dependence of resonant inelastic x-ray scattering: A spherical tensor expansion, Centr. Eur. J. Phys. **12**, 323 (2014)..

[35] F. Borgatti, G. Ghiringhelli, P. Ferriani, G. Ferrari, G. van der Laan, and C. M. Bertoni, Sum rules for resonant inelastic x-ray scattering: Explicit form and angular dependence in perpendicular geometry, Phys. Rev. B **69**, 134420 (2004).

[36] J. Ablett, N. Kordestani, A. Juhin, A. D. Frenza, M.-A. Arrio, P. Rosa, E. Duverger-Nédellec, E. Otero, J.-P. Rueff, P. Sainctavit, and E. Hillard, 1s2p resonant inelastic x-ray scattering natural circular dichroism dataset, Zenodo (2026), https://doi.org/10.5281/zenodo.18648648.